Electronic Supplementary Material (ESI) for Inorganic Chemistry Frontiers.

Supplementary Materials

Structure-property relationships in hybrid: $(C_3H_5N_2)_3[Sb_2I_9]$ and $(C_3H_5N_2)_3[Bi_2I_9]$ isomorphs

M. Węcławik[a], A. Gągor[b], R. Jakubas[a], A. Piecha-Bisiorek[a], W. Medycki[c], J. Baran[b], P. Zieliński[c,d] and M. Gałązka[d]

[a]*Faculty of Chemistry, University of Wrocław, F. Joliot-Curie 14, 50-383 Wrocław, Poland*
[b]*Institute of Molecular Physics, Polish Academy of Science, Smoluchowskiego 17, 60-179 Poznań, Poland*
[c]*Cracow University of Technology, Institute of Physics, Podchorążych 1, 30-084 Kraków, Poland*
[d]*The H. Niewodniczański Institute of Nuclear Physics, PAS, Radzikowskiego 152, 31-342 Kraków, Poland*

TABLE OF CONTENS:

Part 1

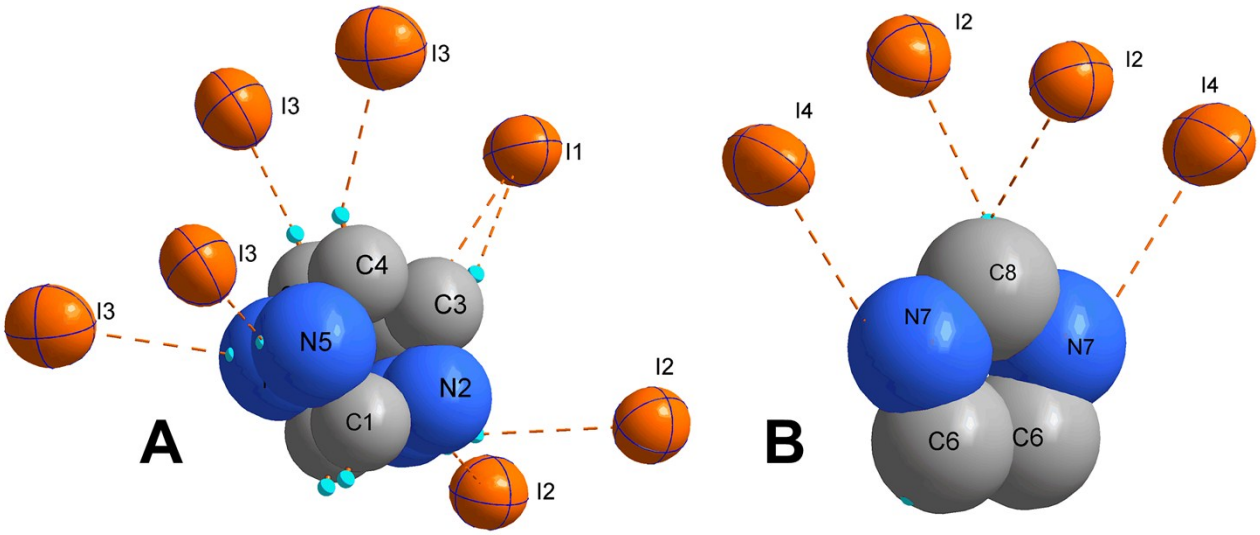

Figure S1. The numbering scheme for Table S1 and ellipsoid representation of the imidazolium A and B, respectively, in the orthorhombic phase II

Table S1. Selected hydrogen-bond parameters for ImIA and ImIB at RT. Bonds involving imidazolium A (yellow) and B (grey) are distinguished and highlighted by the colours of the background.

D—H···*A*	*D*—H (Å)	H···*A* (Å)	*D*···*A* (Å)	*D*—H···*A* (°)	Type of cation
ImIA					
N2—H2···I2	0.86	2.72	3.30 (4)	125.7	A
C3—H3···I1^{i}	0.93	2.62	3.47 (3)	152.7	A
C4—H4···I3^{ii}	0.93	2.68	3.50 (3)	147.2	A
N5—H5···I3^{iii}	0.86	2.83	3.52 (4)	139.1	A
N7—H7···I4	0.86	2.94	3.68 (3)	144.6	B
C8—H8···I2	0.93	3.04	3.76 (4)	135.3	B
C8—H8···I2^{iv}	0.93	3.04	3.76 (4)	135.3	B
ImIB					
C1—H1···I4^{I}	0.93	2.86	3.75 (2)	160.9	A
C4—H4···I3^{III}	0.93	2.82	3.56 (2)	137.5	A
N5—H5···I3^{I}	0.86	2.86	3.56 (3)	140.1	A
N7—H7···I4	0.86	3.03	3.77 (3)	144.4	B

Symmetry code(s): ^{i} *x*+1/2, *y*+1/2, *z*; ^{ii} -*x*+1/2, *y*+1/2, *z*; ^{iii} -*x*+1/2, -*y*+1/2, -*z*+1; ^{iv} -*x*, *y*, -*z*+1/2; ^{I} -*x*+1/2, -*y*+1/2, -*z*+1; ^{III} -*x*+1/2, *y*+1/2, *z*; ^{IV} -*x*, *y*, -*z*+1/2.

Part 2

In Figure S2 one can see that below 90 K a clear deviation of ε from the Cole-Cole plot at frequencies above *ca*. 0.5 MHz takes place. This seems to indicate another dispersion in the megahertz frequency region at low temperatures. Nevertheless, these two relaxators (low frequency (**1**) which is fundamental for this compound and expected higher frequency one (**2**)) are overlapped thus it was impossible to elaborate the dielectric parameters for (**2**).

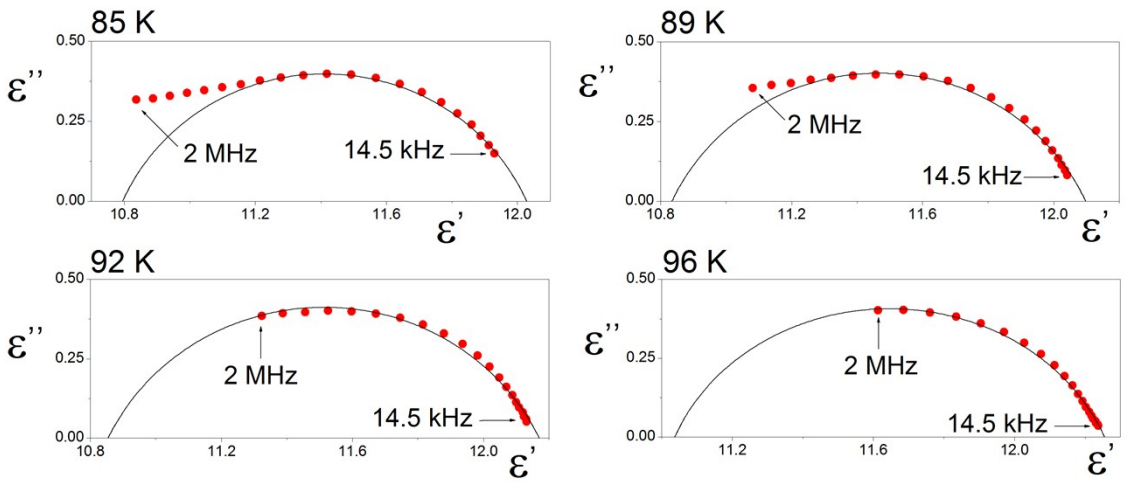

Figure S2. Cole-Cole plots at selected temperatures in ImIB (phase III).

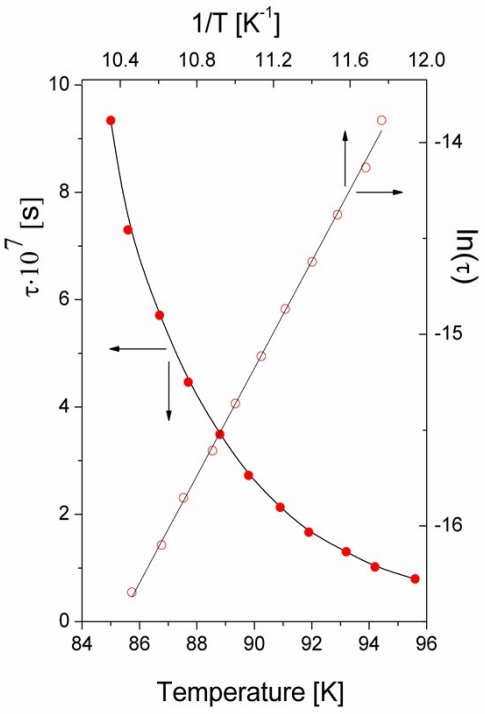

Figure S3 Temperature dependence of macroscopic relaxation time τ versus temperature and ln(τ) versus reciprocal temperature for low frequency relaxator (**1**) for ImIB.

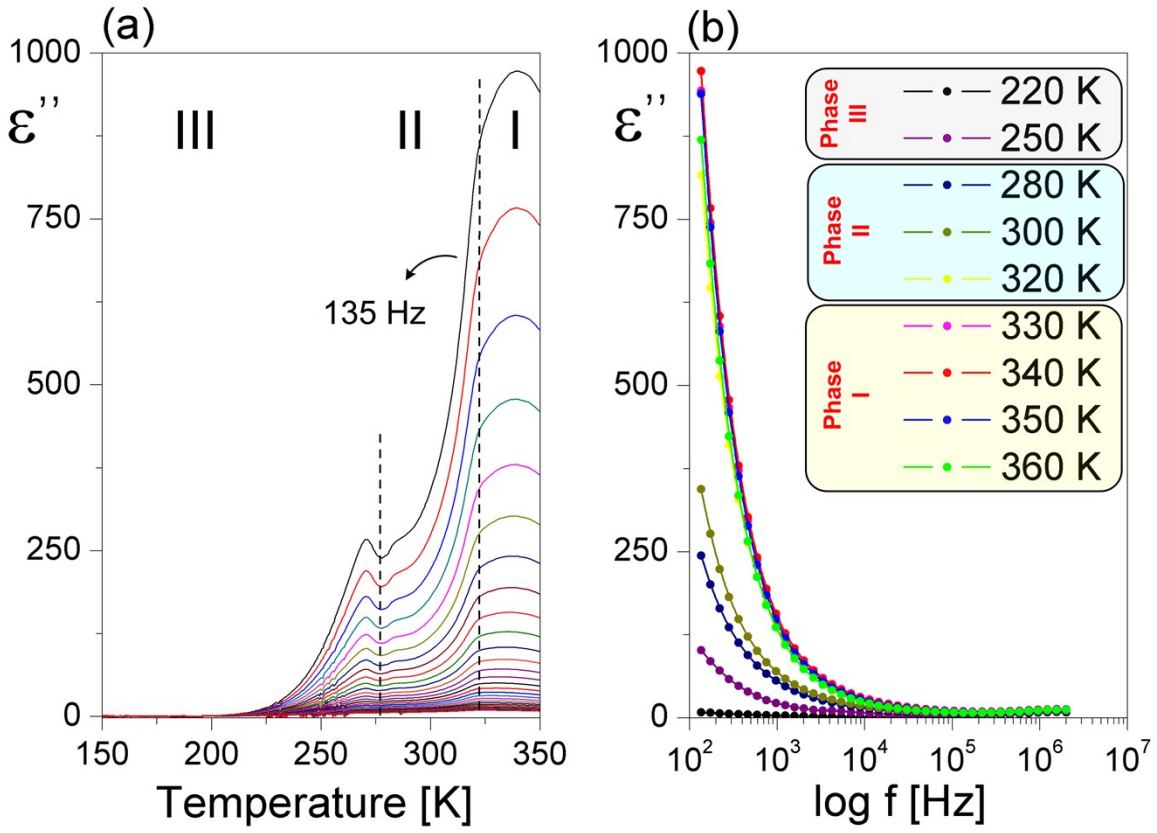

Figure S4. (a) Temperature dependence of the imaginary part (ε'') of the complex dielectric permittivity; (b) Frequency dependence (135 Hz – 2 MHz) of ε'' at various temperatures recorded during heating cycle for polycrystalline sample of ImIA.

Figures S4 (a) and (b) and Figure 5 clearly show the divergence of the complex dielectric permittivity between 350 and 220 K which is mainly due to the conductivity phenomena. The dielectric characteristics presented in Figure S4 (b) do not indicate any relaxation process in ImIA in the analyzed frequency region.

Part 3

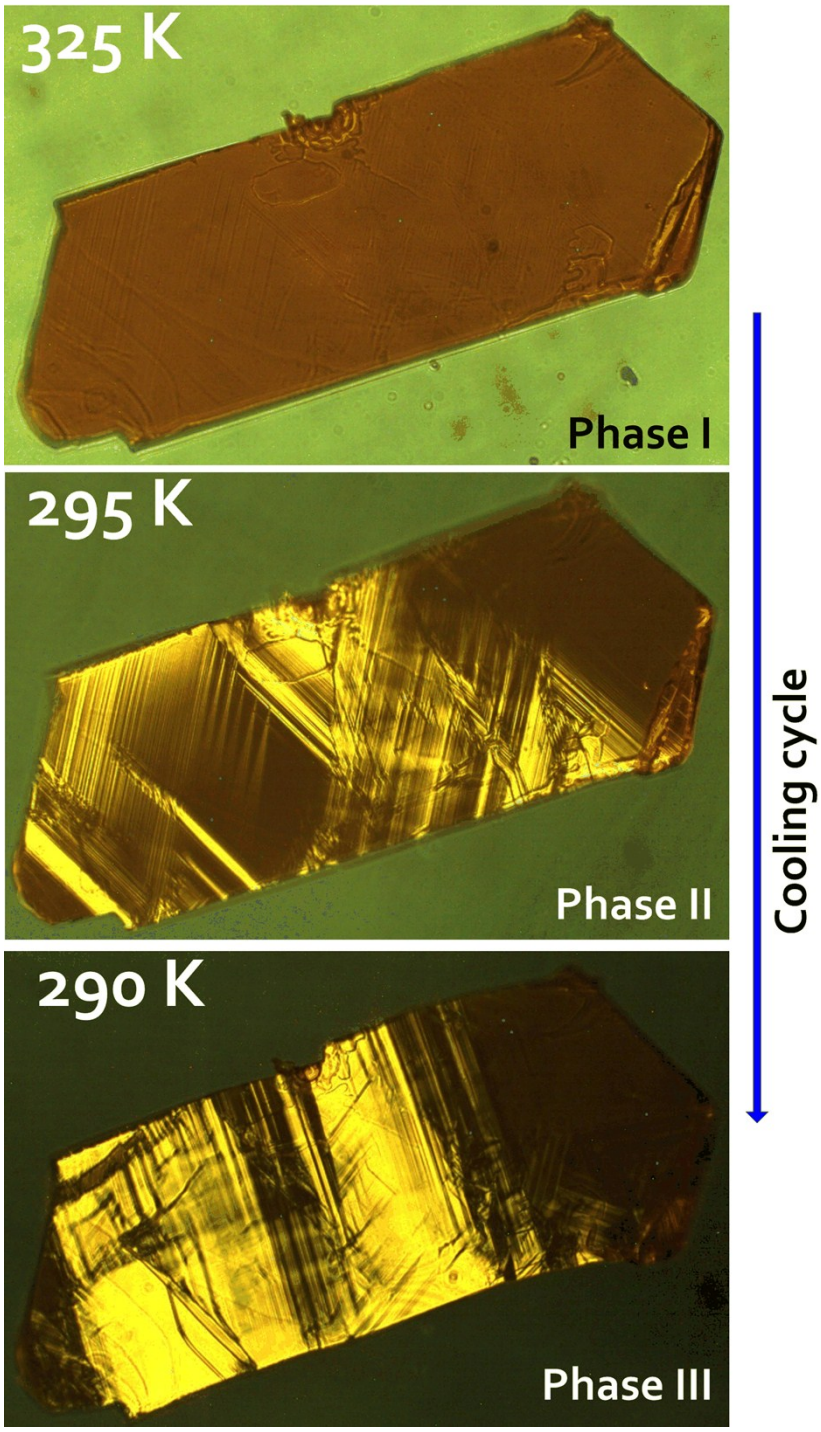

Figure S5 Evolution of the domain structure in ImIB in one cooling cycle

Part 4

The $T_{1(H-H)}$ relaxation rate is given as a combination of spectral densities:[1-5]

$$\frac{1}{T_{1(H-H)}} = C\left(\frac{\tau}{1+\omega_H^2\tau^2} + \frac{4\tau}{1+4\omega_H^2\tau^2}\right), \qquad \text{(eq. S1)}$$

where ω_H is the Larmor proton frequency and C is the relaxation constant:

$$C = (a_{HH}^{DD})^2 = \left(\frac{\gamma^H \gamma^H \mathsf{h}}{r_{H-H}^3}\right)^2 .$$

The other relaxation rates can be obtained the from well-known formulas for the spin–lattice relaxation rate of two different spins:[1-3]

$$\frac{1}{T_{1(H-X)}} = \tfrac{2}{3}(a_{HX}^{DD})^2 \mathrm{l_x}(\mathrm{l_x}+\mathrm{l})\left(\frac{\tau}{1+(\omega_H-\omega_X)^2\tau^2} + \frac{3\tau}{1+\omega_H^2\tau^2} + \frac{6\tau}{1+(\omega_H+\omega_X)^2\tau^2}\right), \qquad \text{(eq. S2)}$$

where: $\omega_{X,}$ (X = N, Sb or Bi, I) are Larmor frequencies of the nuclei in the given compound, a_{HX}^{DD} are the dipole–dipole constants, while $\mathrm{l_N}$ = 1, $\mathrm{l_{Sb(121)}}$ = 5/2, $\mathrm{l_{Sb(123)}}$ = 7/2, $\mathrm{l_{Br}}$ = 3/2. $\mathrm{l_J}$ = 5/2. For simplicity, we assumed the simplest possible form of spectral densities functions with a single exponential dependence of the correlation time versus temperature according to Arrhenius law: $\tau = \tau_0 \exp(E_a/RT)$, where E_a is activation energy.

Table S2 Selected parameters (obtained from eqs. 6 and S1) of three different types of imidazolium cations. Labeling of the cations concerns the lowest temperature phase (III).

Cation	parameter	ImIB	ImIA
1	E_a	1.79 kcal/mol	1.25 kcal/mol
	τ_0	4.27 10^{-13}s	9.65 10^{-12}s
	C_1	5.98 10^{7}s^{-2}	7.13 10^{7}s^{-2}
2	E_a	2.82 kcal/mol	3.22 kcal/mol
	τ_0	6.07 10^{-14}s	3.77 10^{-14}s
	C_2	5.38 10^{8}s^{-2}	5.32 10^{8}s^{-2}
3	E_a	5.21 kcal/mol	5.4 kcal/mol
	τ_0	9.91 10^{-14}s	9.94 10^{-14}s
	C_3	1.05 10^{8}s^{-2}	1.17 10^{8}s^{-2}

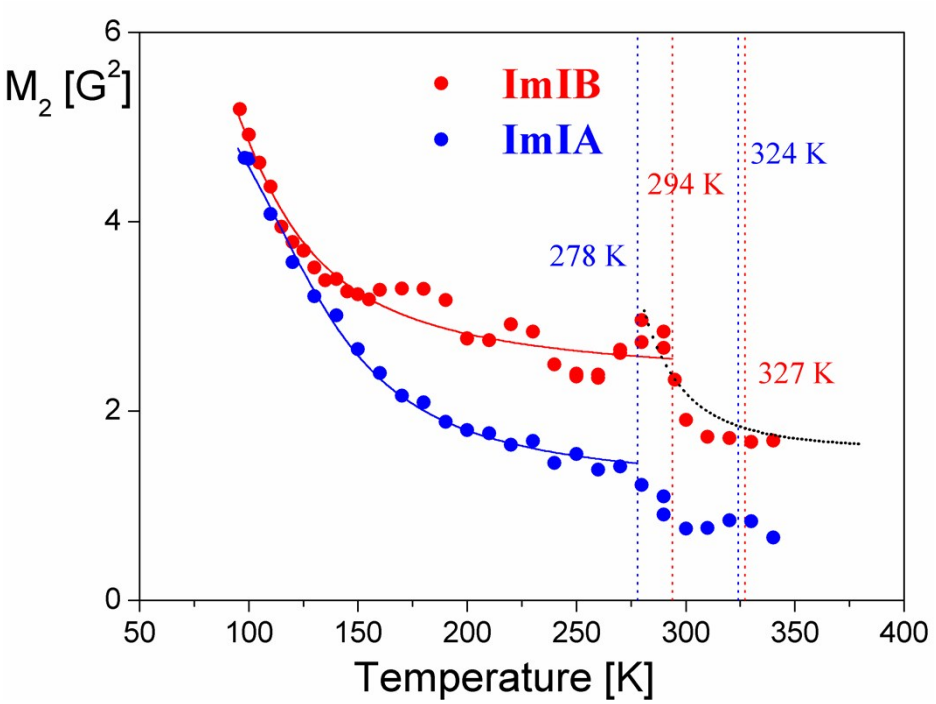

Figure S6. Temperature dependence of second moment of ^{1}H NMR line of ImIA (blue) and ImIB (red).

References:

1 A. Abragam, The Principles of Nuclear Magnetism, Oxford University Press, Oxford, 1961.

2 C. P. Slichter, Principles of Magnetic Resonance, Springer-Verlag, Berlin, 1990.

3 R. R. Ernst, G. Bodenhausen, A. Wokaun, Principles of Nuclear Magnetic Resonance in One and Two Dimensions, Clarendon Press, Oxford, 1994.

4 W. Medycki, K. Holderna-Natkaniec, J. Swiergiel, R. Jakubas, *Solid State Nucl. Magn. Reson*. 2003, **24**, 209.

5 D. Kruk, Theory of evolution and relaxation of multi-spin systems, Application to Nuclear Magnetic Resonance (NMR) and Electron Spin Resonance (ESR), Abramis Academic, Arima Publishing UK, 2007.

Part 5

The infrared spectra of polycrystalline $(C_3H_5N_2)_3[M_2I_9]$, (M = Sb, Bi) in the wavenumbers range between 4000 and 500 cm^{-1} at 300 K (phase II) and 413 K (phase I), and Raman spectra (300 K) are presented in Figures S7-S10. The IR spectra in the frequency range 3000–2800, 1500–1350, 750–700 cm^{-1} are shown as dotted lines as Nujol bands appear in these regions. To cover these areas infrared spectrum in Fluorolube mull at 300 K was measured. Tentative assignments of the observed bands (Table S3) were based on the comparison with imidazole amine.[6-11]

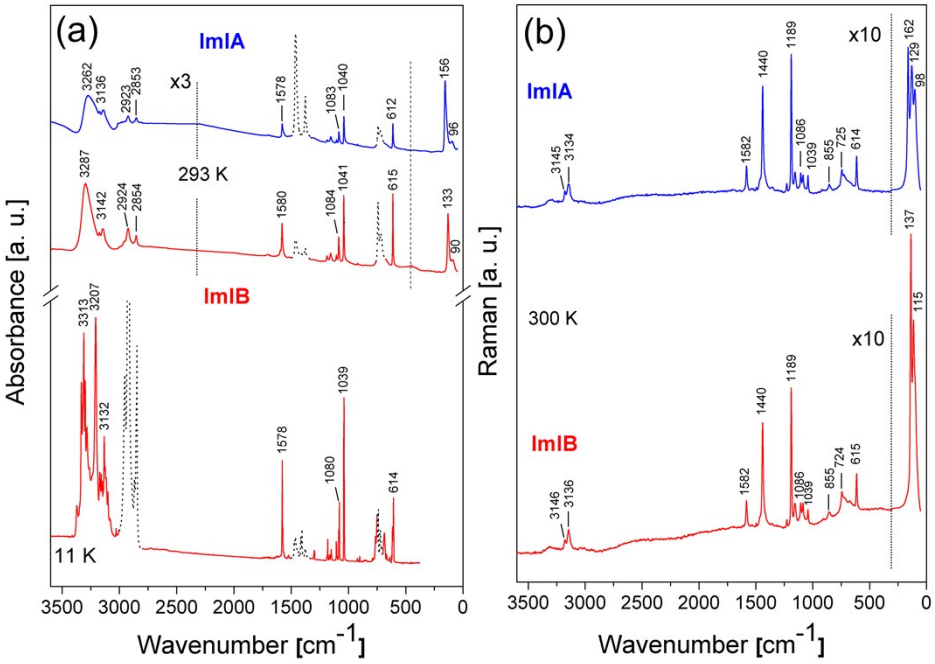

Figure S7. (a) Infrared spectra of powdered ImIA (blue) and ImIB (red) samples in Nujol and Fluorolube (at 300 and 11 K (only for ImIB)); (b) Raman spectra at 300 K.

Experimental details: Powder FT-Raman spectra were recorded with FRA-106 attachment to the Bruker IFS-88 using Nd:YAG diode pump laser. The measurements were performed over the wavenumber range 3500–80 cm^{-1} at room temperature with a resolution better than 2 cm^{-1}.

References:

6 M. Cordes, N. D. J. L. de Walter, *Spectrochim. Acta*, 1968, **24A**, 237.
7 L. Colombo. P. Bleckman, B. Schrader, R. Schneider, Th. Plesser, *J. Chem. Phys*., 1974, **61**, 3270.
8 K. Fan, Y. Xie, J. E. Boggs, *J. Mol. Struct*., 1986, **136**, 339.
9 M. Mojoube, G. Vergoten, *J. Mol. Struct*., 1992, **266**, 345.
10 F. Billes, H. Endredi, G. Jalsovszky *J. Mol. Struct. (Teochem.)*, 1999, **465**, 157.
11 F. Billes, H. Endredi, G. Jalsovszky, *J. Mol. Struct. (teochem)*, 1999, **465**, 157.

Formal classifications of the fundamental modes for ImIA and ImIB

These two crystals posses two phases; hexagonal (phase I) ($P6_3/mmc$ = D_{2h}^4, Z = 2) and orthorhombic (phase II) ($Cmcm$ = D_{2h}^{17}, Z = 4). According to the x-ray data, the $[Sb_2I_9]^{3-}$ anions occupy the D_{3h} sites in the case of phase I and C_{2v} site in the phase II. In both phases, there are two independent types, A and B, of the imidaziolum cations. In the high –temperature phase (I), the A type cations occupy the positions close to C_{3v}(4) sites, whereas the B type cations occupy the positions close to the D_{3h}(2) sites. However, in each case, for both cations there exists a 3-fold disorder, and only one of these positions is occupied by each cation, respectively. Thus, for the A –type cations each of them may occupy one position with the approximate symmetry C_s (the plane symmetry is perpendicular to the plane of heavy atoms), whereas, the B-type cations occupy one of the three possible positions of C_s symmetry, however in this case all atoms lie in the symmetry plane (C_s).

In phase II, the B cations become ordered and occupy the C_{2v} site symmetry. The A type cations still remain disordered and occupy one of two possible positions related by the C_s plane being perpendicular to the a-axis. The highest symmetry of the imidazolium cation is C_{2v} and their normal modes may transform as follows: (9 A_1 (//z, xx,yy,zz) + 3A_2 (i, xy) +8B_1 (//x, zx) + 4 B_2 (//y, yz)). For the Cs symmetry its modes are either 17 A' (//x, //y, xx, yy, zz, xy) + 7 A''(//z, yz, zx), for all atoms lying the symmetry plane, or 13 A' (//x,//y, xx,yy,zz, xy) + 11A'' (//z, yz, zx) for only two atoms (C-H) lying in that plane. Of course, it is also possible that both type of these cations are of C_1 symmetry and all their internal modes (24) are of A type only.

As it follows from the X-ray data, the iodoantimonate(III) anions ($[Sb_2I_9]^{3-}$) are ordered in both phases. They have a face-sharing biooctahedra shape. They occupy the D_{3h} (3m.) site in the high-temperature phase I. They conserve the face-sharing bioctahedral shape in phase II, although their symmetry changes to C_{2v} symmetry. The σ_h plane remains and it is perpendicular to the c-axis; it contains I(1) and two I(2) atoms. The twofold axis is parallel to the b axis and only one atom I(1) lies on it, The second mirror plane is perpendicular to the a-axis and it contains two Sb atoms, I1 and two I4 atoms. The internal modes of the iodoantimonate(III) anions of D_{3h} site symmetry can be classified as $4A_1$(xx+yy,zz) + A_2' + 5E' (X,Y; xx-yy,xy) + A_1'' + $3A_2''$(Z) +4E''(yz,zx), among which 8 modes (5E' + $3A_2$) are IR active and 13 ($4A_1$+ 5E'+ 4E'') are Raman active. The internal modes for the iodoantimonate(III) anions of C_{2v} site symmetry can be classified as: $9A_1$ (Z; xx,yy, zz) + $5A_2$ (xy) + $6B_1$ (X, zx) + 7 B_2(Y; yz); all of them are allowed in Raman (27 modes) and only 22 are allowed in the IR spectra. Thus, one can expect significant differences between the vibrational spectra (IR and Raman) of the title crystal measured in these two phases.

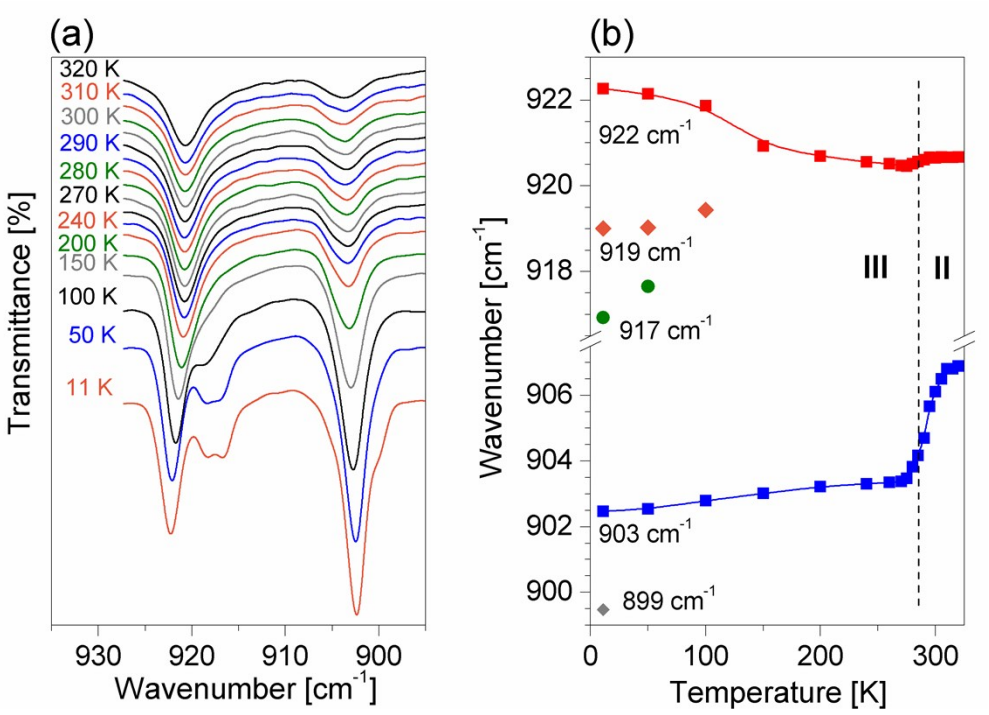

Figure S8. (a) Infrared spectra between 895 and 925 cm^{-1} of the ImIB as functions of temperature, (b) plot of the wavenumber β(R), β(CH) mode frequencies of ImIB as a function of temperature (R-ring).

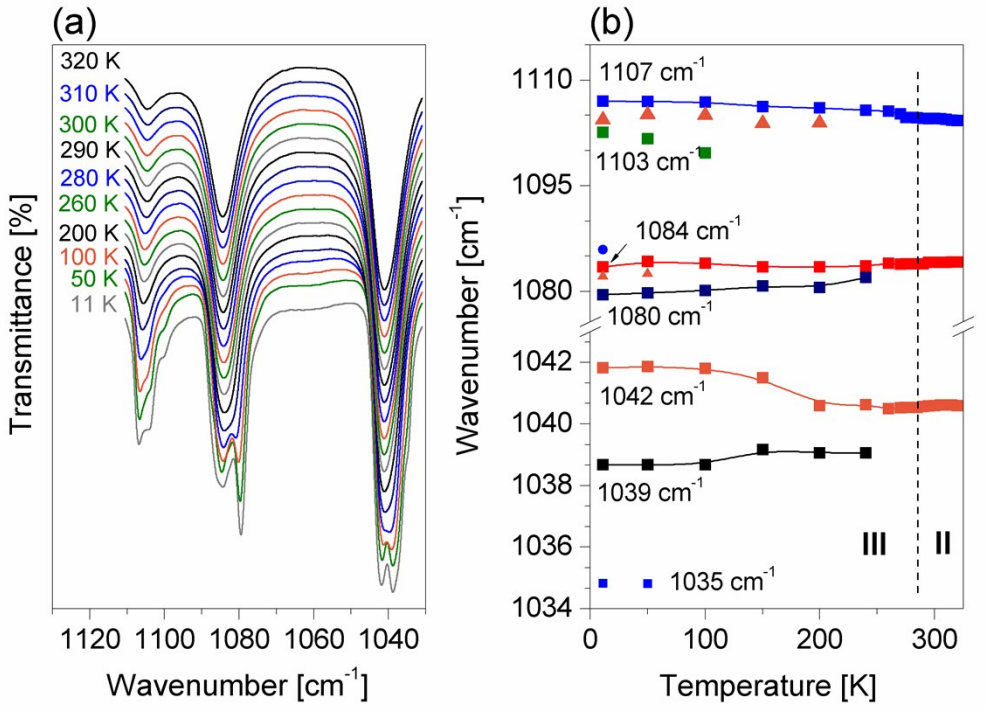

Figure S9. (a) The infrared spectra between 1030 and 1110 cm^{-1} of the ImIB as functions of temperature, (b) plot of the ν(R) δ(CH) mode frequencies of ImIB as a function of temperature.

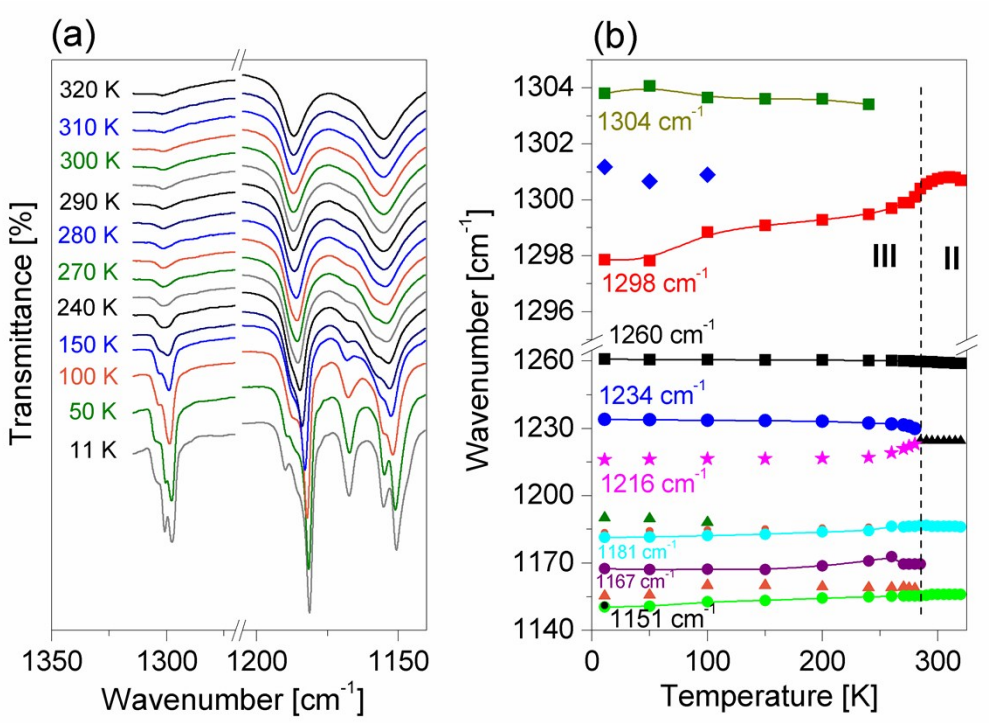

Figure S10. (a) The infrared spectra between 1140 and 1310 cm^{-1} of the ImIB as a function of temperature, (b) plot of the Ring breathing, ν(R), β(CH) mode frequencies of ImIB as a function of temperature.

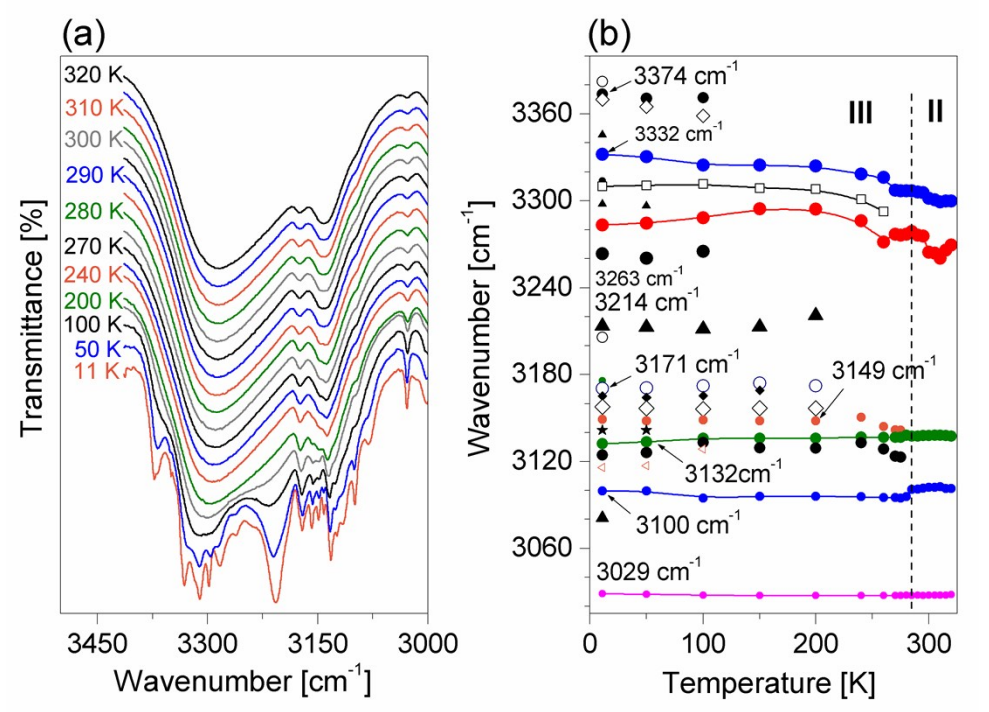

Figure S11. (a) The infrared spectra between 3000 and 3400 cm^{-1} of the ImIB as functions of temperature, (b) plot of the ν(NH) mode frequencies of ImIB as a function of temperature.

Table S4 .

Wavenumbers (cm^{-1}) and relative intensities of the bands observed in the Infrared and Raman spectra of ImIB and Raman at 293 K) and ImIA (IR and Raman at 293 K). IR spectra as functions of temperature were measured for the emulsion in Nujol in between CsI windows.

IR			Raman		Assignments[11]
ImIB		ImIA	ImIB	ImIA	
11 K	293 K	293 K	293 K	11 K	
	3492 vw				
3382 sh m	3287 vs				
3374 w					ν(NH)
3369 sh m					
3345 sh m					
3332 s					
3313 s sh					
3310 s			3305 vw	3308 vw	
3298 m					
3283 m					
3263 m		3262 s			
		3241 vw			
3214 m					
3235 m sh					
3207 s sh					
3195 s sh		3202 vw			
3176 sh m	3173 w	3172 w	3178vw	3178 vw	ν(CH)
3171 m					
3158 m					
			3146 vw	3145 vw	
3149 m	3150 vw				
3142 m	3142 m				
3132 s	3139 vw				
3124 m	3138 vw	3136 m	3136 vw		
3116 m				3134 vw	
3100 m	3100 m sh	3108 vw			
3081 w					
3030 vw sh					
3029 m	3029 vw				
	2964 w	2964 vw			
	2902 vw				Overtones
	2872 vw				
		2861 vw			
	2854 m				
		2853 m			
		2730 vw			
		2592 vw			
	2457 vw				
	2403 vw				
	2383 w	2380 vw			
	2349 vw				

		2346 vw			
	2303 m				
	2266 vw				
	2205 vw				
		2188 vw			
	2146 vw				
	1779 vw				
	1745 m	1744 w			
	1708 vw	1703 vw			
		1654 vw			
	1607 vw sh	1606 vw			
1595cvw	1596 sh vw				
1582 vs sh	1580 m		1582 vw	1582 vw	
1578 vs	1578 m	1578 s			ν(R)+β(CH)+β(NH)
1574 w sh					
1566 vw	1567 vw sh				
		1549 vw	1534 vw	1534 vw	
1526 vw					
1522 vw		1522 w			
		1499 vw			
		1491 vw			
1465 s sh		1480 vw			ν(R)+β(CH)
1461 vs			1460 vw sh	1460 vw sh	
1457 s sh					
1455 s sh					
	1441 w		1440 w	1440 w	ν(R)+β(CH)+β(NH)
	1414 vw				
1416 m		1410 vw			
1406 m	1406 vw				
		1400 vw			
		1378 s			ν(R)+β(CH)
		1365 w			
		1352 vw	1358 vw	1358 vw	
		1342 vw			
		1315 vw			
1304 w sh	1301 vw	1302 vw			Ring breathing
1301 m					ν(R)+β(CH)
1298 m					
1260 vw	1262 vw				
1234 vw sh	1228 vw		1228 vw	1228 vw	
1216 vw					
1190 w	1187 w				
1185 w sh		1187 w	1189 w	1189 w	
1181 s					
1167 w	1167 vw				ν(R)+δ(CH)
1155 m	1155 w		1156 vw	1155 vw	
1151 m		1154 w			
1150 w sh					
1107 m	1104 vw	1105 vw	1105 vw	1106 vw	
1105 m					
1103 w sh					

1086 m sh	1084 m	1084 m			
1084 s			1086 vw	1086 vw	
1083 m sh					
1080 vs					
	1050 vw sh		1043 vw	1042 vw	
1042 vs	1041 vs	1040 vs	1039 vw	1039 vw	
1039 vs					
1035 s sh					
		1030 vw			ν(R)+β(CH)+β(NH)
		1016 vw			
	965 vw	978 vw			
922 w	921 vw	920 vw			
919 vw					
917 vw			911 vw	911 vw	
903 w	904 vw				
899 vw sh					
893 vw					β(R)+β(CH)
890 vw sh					
888 vw					β(R)
871 w					γ(CH)
866 vw sh					
862 w					
860 w			855 vw	855 vw	
854 w					
852 w					
849 vw					
	851 vw				ω(CH)
843 vw					
794 vw					
780 vw					
765 m					
757 s sh					
750 s					
740 s	744 vs	756 w	743 vw	742 vw	
733 w					
689 s					τ(R)
686 s					
680 m sh					
668 vw		668 vw	674 vw		
654 vw					
650 vw					τ(R)
641 w		642 vw			
639 w					
634 vw sh					τ(R)+ω(NH)
625 w sh					
623 vw					
617 s	615 vs				
614 s					
611 s		612 vs	615 vw	614 vw	
608 vs					

606 s sh					
	326 vw				ν(Bi/Sb-I)terminal
		218 vw			
	203 vw				
		160 vw			ν(Bi/Sb-I)bridged
		156 vs		162 vs s	
		137 w			
	133 vs		137 vs		
				129 s	
	122 s				
			115 s	103 s	δ(I-Bi/Sb-I)
		112 w	103 s sh		
	99 s				
				98 m	
		96 s			
	90 s				Lattice vibrations
		72 w			

Legend: vs – very strong; s – strong; m – medium, w – weak, vw – very weak, sh – shoulder; ν - stretching; δ - in-plane bending (scissoring); ω - out-of-plane bending (wagging); τ - out-of-plane bending (twisting); β in-plane bending; R –ring.